Received: 28 September 2021 | Revised: 28 February 2022 | Accepted: 18 April 2022

DOI: 10.1002/stc.2987

RESEARCH ARTICLE

WILEY

Tandem tuned mass damper inerter for passive control of buildings under seismic loads

Maziar Fahimi Farzam[1] | **Himan Hojat Jalali**[2]

[1]Faculty of Engineering, University of Maragheh, Maragheh, Iran

[2]Department of Civil Engineering, University of Texas at Arlington, Arlington, Texas, USA

Correspondence
Maziar Fahimi Farzam, Faculty of Engineering, University of Maragheh, Iran.
Email: m.farzam@maragheh.ac.ir

Summary

Tuned mass damper inerter (TMDI) is becoming a well-known device for mitigating structural vibrations. However, to be effective, the inerter needs to be connected to lower stories, which can interfere with the architectural features and therefore limit its feasibility. To overcome this challenge, a rooftop tandem tuned mass damper inerter (TTMDI) device for the structural control of a well-recognized benchmark 10-story shear building is proposed, in which the mass of the conventional TMDI is divided into two variable masses that are connected to each other using a spring and dashpot. The seven TTMDI free parameters (frequency and damping ratio of the two masses connected to the roof, the frequency and damping ratio of the connected masses, and their relative mass ratio) are optimized using particle swarm optimization algorithm (PSO) by minimizing the largest singular value of story drift transfer function. To evaluate the robustness of the optimal damper, its performance is compared to two comparable tuned TMDI configurations (TMDI-9 and TMDI-8) in both frequency and time domains under 21 far- and near-field records with forward directivity (FD) and fling step (FS) for a preselected mass ratio of 1% and three different inertance ratios. The performance indices in the time domain were selected as the maximum story drifts and absolute story acceleration. Results show that the rooftop TTMDI outperforms both TMDI configurations in both frequency and time domains, and its performance is more robust in terms of not exceeding the uncontrolled responses for most of the considered earthquake records.

KEYWORDS

inerter, particle swarm optimization, structural control, time history analysis, tuned mass damper

1 | INTRODUCTION

It has been almost 50 years since the passive tuned mass damper (TMD) has been recognized as an efficient and reliable device in controlling the vibration of tall buildings against wind and has been practically implemented in many tall buildings around the world. Since then, the similarities between wind and earthquake loads as the main dynamic lateral loads affecting the design of tall buildings have shaped extensive research efforts to evaluate the seismic performance of TMD and improve its performance against natural ground motions.[2,3] However, due to the main differences

between these dynamic lateral loads and especially the difference in their frequency contents, the seismic performance of TMD is still being debated, and improving its seismic efficiency is an active research topic in the structural control community.[4–6]

Frahm[7] proposed the idea of an additional mass to reduce the vibration of an undamped main system in 1909, more than 110 years ago (Figure 1a). The evolution of the TMD is presented in Figure 1, in which M, C, and K are the mass, stiffness, and damping coefficient of the main structure, respectively, while m_d, c_d, and k_d are the mass, stiffness, and damping coefficient of the TMD, respectively; X_d, X_g, and $\ddot{X}_g$ are the displacement vectors of the added mass, the ground displacement, and accelerations, respectively. The three major issues of efficiency, robustness, and simplicity of construction have always been the focus of researchers in the development of TMDs. Usually, it is not possible to improve all three features simultaneously; however, due to the trade-off between these features, it seems that providing a balance between them would be the best possible design. Therefore, over the past decades, several modifications of TMD have been attempted to bring all three features to an acceptable level. About 5 years after Frahm's patent, i.e., the idea of an additional mass with a spring, Lanchester[8] significantly improved the TMD robustness by replacing the spring with a viscous damper (Figure 1b). However, the efficiency of this new device was scarified compared to Frahm's idea, especially in the tuning frequency. Furthermore, den Hartog[9] combined the two ideas of Frahm[7] and Lanchester[8] to improve both performance and robustness at the same time (Figure 1c). In addition to combining these two ideas, he also regulated a framework for determining the optimum parameters of the damper, which had already been addressed by previous researchers. In this framework, three parameters of mass, damping, and frequency ratios are selected to be the optimum TMD design parameters, represented by μ, ζ_d, and f_d, respectively, as defined in Equation (1). The mass ratio is conventionally preselected based on construction limitations, while the damping and frequency ratios are assumed as optimization variables. Figure 1d shows the final configuration of the currently recognized TMD.

$$\mu = \frac{m_d}{\mathrm{M}};\ \zeta_d = \frac{c_d}{2m_d\omega_d};\ f_d = \frac{\omega_d}{\omega_s} = \frac{\sqrt{\frac{k_d}{m_d}}}{\sqrt{\frac{K}{M}}} \tag{1}$$

Consequently, due to the lack of development of computational tools, the optimum design to simultaneously improve efficiency, and robustness was performed using analytical or quasi-analytical methods. Therefore, the studied systems were limited to structures without damping or with small inherent damping. Thereafter, in the computer era and with the emergence of the metaheuristic algorithms, this limitation was completely overcome, and the optimal design of any configuration became practical (Figure 1d).

In the early 1970s, researchers found that the passive TMD in its classical form did not seem to perform adequately under earthquake loads and were, therefore, looking for new alternatives. To this end, active and semi-active (smart devices) control theories were developed and proposed by researchers in the structural control community (Figure 2).[10] Although these approaches were sound and worked quite promising initially, the added cost of equipment, advanced

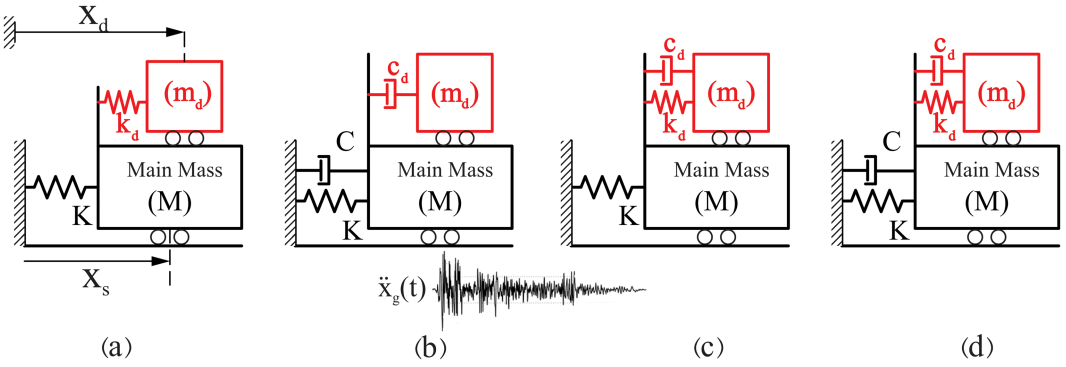

FIGURE 1 Development history: (a) primary proposition concept of Frahm,[7] (b) primary proposition concept of Lanchester,[8] (c) milestone modification of Den Hartog,[9] and (d) physical realization model of Warburton

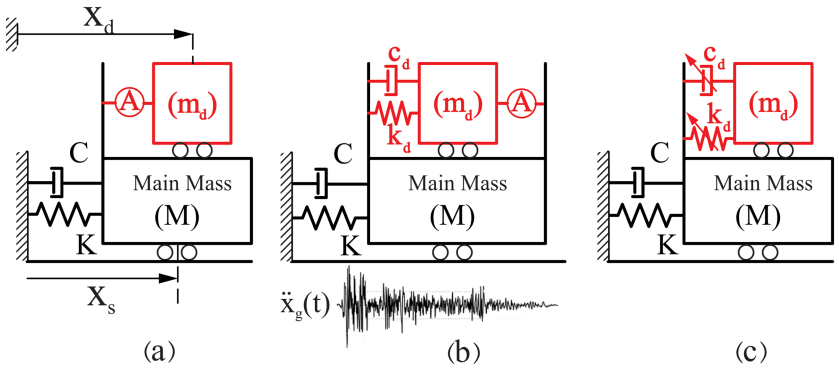

FIGURE 2 Smart configurations: (a) active mass damper,[11] (b) active tuned mass damper,[12] and (c) semi-active TMD[13]

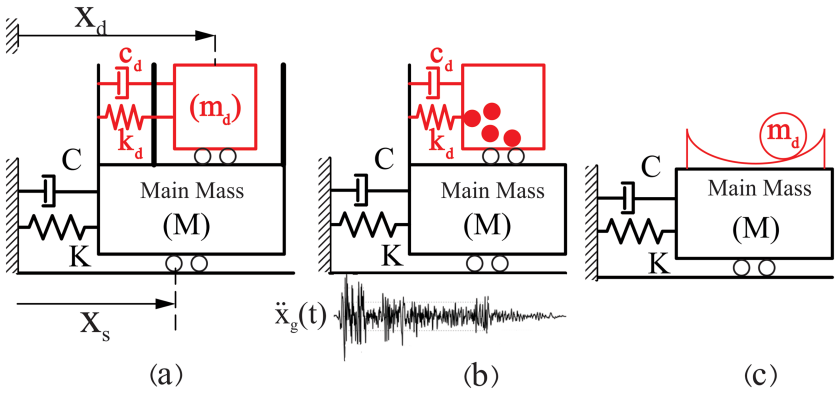

FIGURE 3 Nonlinear configurations: (a) pounding TMD,[14] (b) particle TMD, and (c) pendulum TMD[16]

technology, high maintenance costs, the need for an external energy source, high expertise required for components, etc. were some of the major drawbacks that made these devices less competitive when compared to passive devices.

On the other hand, studies have shown that increasing the mass ratio in a classical mass damper can significantly improve its robustness and performance, and unorthodox configurations have therefore been proposed for the implementation of such systems.[4,5] But the construction difficulties of securing and accommodating a large mass ratio have been a serious obstacle to the application of this modification. More recently, nonlinear vibration absorbers have been studied, which exhibit good performance due to increasing the effective frequency band.[14] However, due to the need for nonlinear modeling, the evolution of these devices has been slow. Figure 3 shows some examples of nonlinear vibration absorbers including the pounding TMD[14] (Figure 3a), particle TMD[15] (Figure 3b), and pendulum TMD[16] (Figure 3c).

In the meantime, the introduction of a linear instrument by Smith in 2002,[17] i.e. the inerter, which creates an apparent mass that could solve the large real mass requirement, quickly caught the attention of the control engineering community. As a linear massless instrument, the inerter develops a force proportional to the relative acceleration through the inertance constant, *b*, as shown in Figure 4a. Although there is no consensus on the first use of the inerter concept in structural control,[19] in the last decade, various inerter configurations have been introduced and studied as new and promising devices for structural control, e.g., the Tuned Viscous Mass Damper (TVMD),[20] Tuned Mass Damper Inerter (TMDI),[21] and Tuned Inerter Damper (TID)[22] (Figure 4). Among these, TMDI most closely resembles the classic TMD, and any improvement of it can be used to design more efficient new TMDs, as well as update previously implemented TMDs that are sensitive to detuning effects.

The original TMDI on single-degree-of-freedom (SDOF) structure was proposed by Marian and Giaralis,[21] in which the two inerter terminals were connected to the auxiliary mass and the ground and exhibited outstanding performance in its particular grounded TMDI (GTMDI) configuration. Previous research has shown that the introduction of inertance in the TMDI is accompanied by two opposite characteristics of negative stiffness and mass amplification effects.[18,23] In the case of GTMDI, the presence of the inerter improves the response due to pure mass amplification effects. However, the use of rooftop TMDI in a multi-degree-of-freedom (MDOF) requires an inerter connection to the

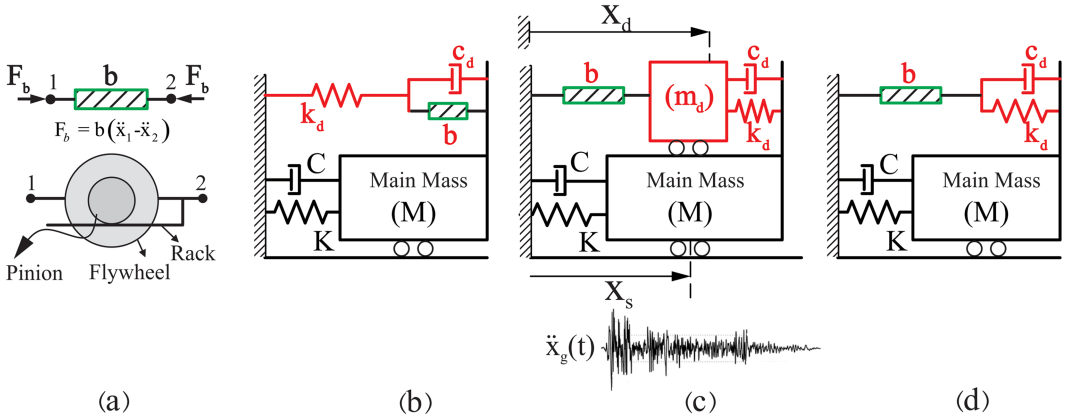

FIGURE 4 Inerter-based configurations: (a) ideal inerter with rack and pinion realization,[18] (b) TVMD,[20] (c) TMDI,[21] and (d) TID[22]

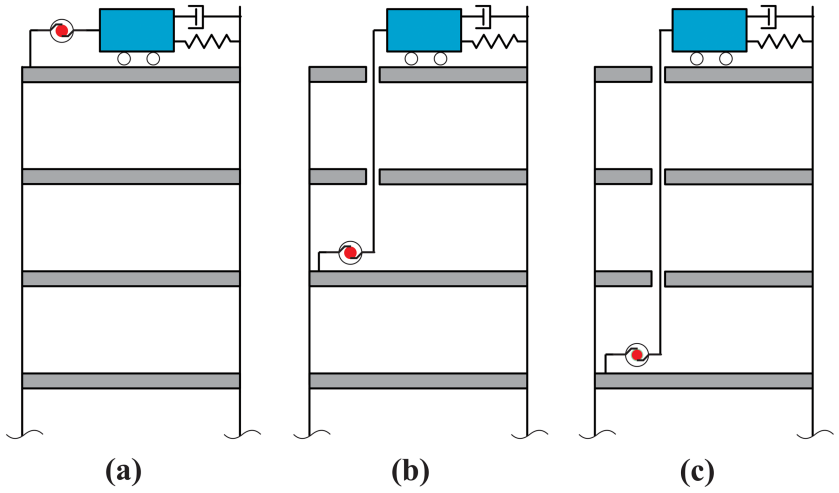

FIGURE 5 Schematic illustration for rooftop TMDI with the second terminal of inerter connected to (a) roof, (b) two stories lower, and (c) three stories lower

upper floors due to lack of ground access (Figure 5a). In this case, the addition of inertance imposes both negative stiffness and mass amplification effects, which can have negative/positive effects on the control performance of TMDI depending on which one prevails. Negative stiffness reduces the efficiency of the rooftop TMDI, while mass amplification enhances its performance. Furthermore, increasing the inertance (b) can exacerbate both the negative stiffness and mass amplification effects.[23,24] Kaveh et al.[25] showed that by connecting the second terminal of the rooftop TMDI to the roof, the TMDI-controlled building performs similar to an uncontrolled building. However, by lowering the second terminal and connecting it to the lower floors (Figure 5b,c), the efficiency of this system will gradually improve due to the correlation reduction and the increase of relative motion between the responses of the two ends of the inerter. This has also been recognized by other research,[24,26–28] where it has been shown that TMDI performance is continuously improved by increasing the distance between the floors that the terminals of the inerter are connected to (inerter location parameter) due to prevailing mass amplification over negative stiffness effects. However, lowering the second terminal of the inerter generally will interfere with the architectural features and has been a serious obstacle to the application of this system.

Furthermore, some recent studies have shown that in structures whose responses are dominated by the first mode, the TMDI performance is directly related to the difference of modal shape values between the two floors that the inerter terminals are connected to; in other words, the larger the difference between the two modal shape values of the inerter terminals, the better the TMDI performs, especially for low mass ratios.[23,24] The inerter location parameter, $\Delta\varphi$, is defined as the difference between modal values of the roof and story k, $\Delta\varphi = (1 - \varphi_k)$, with φ_k

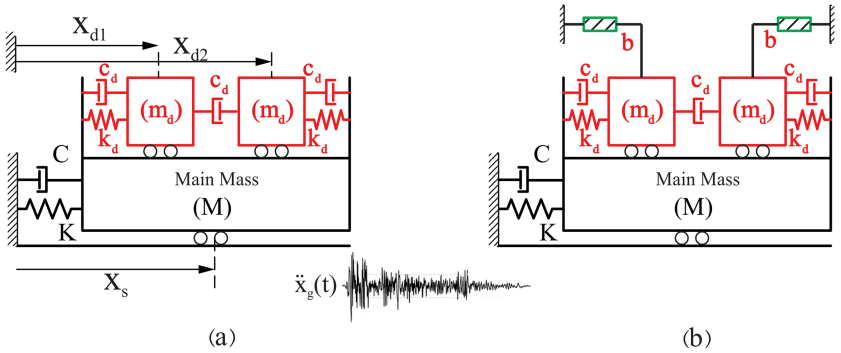

FIGURE 6 Tandem-based configurations: (a) tuned tandem mass damper (TTMD)[31] and (b) tuned tandem mass damper inerter (TTMDI)[32]

being the value of the modal shape at story k normalized to the roof modal shape value. Due to the important role of this parameter among other damper design parameters, increasing $\Delta\varphi$ has been considered either directly (by connecting the second terminal of the inerter as farthest away from the rooftop, which creates architectural issues)[24,26–28] or indirectly (by changing the modal shape of structures through manipulating the design of the structure).[29,30] In the indirect approach, any modification in the structural or damper configuration that can magnify $\Delta\varphi$ by generally increasing the curvature of the modal shape[29] or by locally increasing the modal shape difference between the two floors that the inerter terminals are connected to[30] can be very effective in improving the performance of the rooftop TMDI.

Recently, Yang and Li,[31] as well as Cao and Li,[32] have discussed the idea of tandem tuned mass dampers (TTMDs) (Figure 6) alone and in combination with inerter, respectively. In both studies, a single degree of freedom structure has been studied, and, in the latter, the second inerter terminal is connected to the ground. It seems that using the idea of tandem mass for a rooftop TMDI can be beneficial, since one of the masses can act as a controllable "dummy" story, virtually increase the distance between the two inerter terminals, and increase $\Delta\varphi$ locally, which may help to ease the implementation of TMDI.

In this study, a new rooftop tandem tuned mass damper inerter (TTMDI) configuration, inspired by the idea of Cao and Li,[32] is proposed in which the tandem variable masses are connected to each other using a spring and dashpot, and unlike the configuration of Cao and Li,[32] only one of the masses is connected to an inerter device. As mentioned earlier, the purpose of dividing the total mass of a rooftop TMDI is virtually increasing the distance between the two terminals of the inerter by allocating part of the mass to create a controllable dummy floor, which would potentially result in a change in modal shape values, without interfering with architectural features in the lower stories. However, the ratio between the two masses was considered as a design variable to come up with an optimized solution. The proposed TTMDI is employed for the optimal structural control of a benchmark 10-story linear shear building with 2% inherent damping ratio, and its efficiency and robustness are evaluated in both frequency and time domains under a suitable set of far- and near-field records. To better assess the performance of the proposed TTMDI, results are also presented for comparable TMDI configurations, i.e., TMDI-9 and TMDI-8, for which the second terminal of the inerter is connected to the 9th and 8th stories, respectively.

The remainder of the paper is structured as follows. In Section 2, the characteristics of the benchmark 10-story shear building and the governing equations of motion of a TMDI-/TTMDI-equipped N-story shear building are established. Additionally, the definition of objective function, the definition of preselected and design variables, their admissible domain, and the seismic record information used for performance evaluation in time domain are presented in Section 2. Section 3 discusses the optimum values of the TMDI/TTMDI tuning parameters based on the selected objective function and their performance in the frequency domain. In Section 4, the performance of the optimally controlled structure is evaluated in the time domain under 21 far-field and near-field earthquakes with forward directivity (FD) and fling step (FS) characteristics based on two well-appreciated performance criteria, i.e., story drift and absolute story acceleration. In the last section, the concluding remarks and the possible future research directions are outlined. Finally, the different matrices used in the equation of motion are included in the appendix.

2 | MODELS AND METHODS

To optimally design the introduced control device (TTMDI) and simultaneously compare its efficiency and robustness with the well-recognized rooftop TMDI configurations, a 10-story benchmark shear building is considered in this study.[2,33–35] The building has been widely used in research studies by the control community. Table 1 presents the dynamic properties of the 10-story shear building.

A 2% inherent damping is assumed as a common damping ratio, which in many dynamic analyses are preferred as the equivalent viscous damping ratio for the buildings. Considering the n-story linear shear building with rooftop TMDI, the state space equation of motion subjected to earthquake can be written as shown in Equation (2).

$$\dot{\boldsymbol{Z}}(t) = \mathbf{A}\mathbf{Z}(\mathrm{t}) + \mathbf{B}\ddot{\mathrm{x}}_g(t), \tag{2}$$

where $\ddot{x}_g(t)$ is the ground acceleration and **A**, **B**, and **Z** are the system matrix, location matrix, and the state vector, respectively, as shown in Equation (3).

$$\mathbf{Z}(\mathrm{t}) = \begin{bmatrix} \mathbf{X}(\mathrm{t}) \\ \dot{\mathbf{X}}(\mathrm{t}) \end{bmatrix}, \mathbf{A} = \begin{bmatrix} \mathbf{0} & \boldsymbol{I} \\ -\boldsymbol{M}^{-1}\boldsymbol{K} & -\boldsymbol{M}^{-1}\boldsymbol{C} \end{bmatrix}, \mathbf{B} = \begin{bmatrix} \mathbf{0} \\ \boldsymbol{M}^{-1}\boldsymbol{h} \end{bmatrix}. \tag{3}$$

X and $\dot{\mathbf{X}}$ are the $(n + x)$ dimension relative displacement and velocity of each degree of freedom (DOF) with respect to the ground; $\boldsymbol{M}$, $\boldsymbol{C}$, and $\boldsymbol{K}$ are $(n + x \times n + x)$ matrices corresponding to the mass, damping, and stiffness of the uncontrolled/controlled shear building, respectively, where $n = 10$, $x = 0$ for uncontrolled, $x = 1$ for TMDI, and $x = 2$ for TTMDI; $\boldsymbol{0}$ and $\boldsymbol{I}$ are the zero and identity matrices, respectively; $\boldsymbol{h}$ is a vector containing the masses of the degrees of freedom of the system and is presented along with the mass, stiffness, damping, and other matrices for the TMDI/TTMDI-equipped building in the appendix. The transfer function of the governing equation of motion is shown in Equation (4).

$$\mathbf{G}(s) = \mathbf{C}_{\boldsymbol{y}}(\mathrm{j}\omega\mathbf{I} - \mathbf{A})^{-1}\mathbf{B}, \tag{4}$$

where "j" is defined as $\mathrm{j} = \sqrt{-1}$; ω is the circular frequency content; and C_y is dependent on the type of response measurement and for story drift is defined as Equation (5).

$$\mathbf{C}_{\boldsymbol{y}} = \begin{bmatrix} \begin{bmatrix} 1 & & & & \\ -1 & 1 & & \mathbf{0} & \\ & -1 & 1 & & \\ & & & \ddots & \\ \mathbf{0} & & & -1 & 1 \\ & & & & -1 \end{bmatrix}_{n\times n} & \mathbf{0}_{n\times(n+2x)} \end{bmatrix}_{n\times 2(n+x)}. \tag{5}$$

In this case, G(s) is multiple input-multiple output model, and the H_∞ norm is defined by Equation (6). It should be noted the TMDI/TTMDI motion should not be considered in Equation (6).

TABLE 1 Structural parameters of the 10-story benchmark building[2,33–35]

Story	1	2	3	4	5	6	7	8	9	10
Mass ($\times 10^3$ kg)	179	170	161	152	143	134	125	116	107	98
Stiffness ($\times 10^6$ N/m)	62.47	59.26	56.14	53.02	49.91	46.79	43.67	40.55	37.43	34.31

$$\|\mathbf{G}(s)\|_{\infty} = \max_{\omega} \sigma_{max}(\mathbf{G}(j\omega)), \tag{6}$$

where $\sigma_{max}(.)$ is the largest singular value of the transfer function.

Figure 7 shows the considered configurations for the current study, i.e., TMDI-9 (Figure 7a) and TMDI-8 (Figure 7b), in which the second terminal of the inerter are connected to the 9th and 8th stories, respectively, and the newly proposed TTMDI-9, where the first terminal of the inerter is connected to the second rooftop added mass and the second terminal of the inerter is connected to the 9th story (Figure 7c). The first mass, m_{d1}, which can act as a controllable dummy floor, is colored in blue to better distinguish it from the second mass, m_{d2}, which is connected to the inerter. The two masses of the TTMDI assign additional anti-resonance in comparison to TMDI, which could allow for additional control over the damper performance.[36] Additionally, full connecting elements of spring and damper between the two added masses are assumed to provide more design flexibility for the proposed device, and the decision on redundant connections is left to the metaheuristic algorithm.

Table 2 summarizes a set of dimensionless preselected variables, design variables, and their studied ranges for the aforementioned cases in Matlab. The design parameters of TTMDI include inertance ratio, β; total mass ratio (TMR), $\mu_1 + \mu_2$; relative mass ratio (RMR), μ_1/μ_2; and the damping and frequency ratios of the 1st mass (ζ_{d1} and f_{d1}), the 2nd mass (ζ_{d2} and f_{d2}), and their connection (ζ_{dc} and f_{dc}). Similarly, the four design parameters of TMDI include inertance ratio, β; the mass ratio, μ; and the damping and frequency ratios of the only mass (ζ_d and f_d). The inertance and total mass ratios are assumed as preselected parameters for both the TMDI and TTMDI, while the damping and frequency ratios are taken as design variables. Additionally, since the TTMDI has two masses to enhance design flexibility, the RMR is also selected as a design variable in this damper, resulting in a total number of seven design variables. In Table 2, $\overline{m}$ represents the average of the tandem masses.

The objective function for the optimization problem is minimizing the H_∞ norm of maximum story drift ($\|\mathbf{G}(s)\|_{\infty}$) as a measure for damage to structural and non-structural components. Given that the objective function is defined as the minimization of the largest singular value of the story drift transfer function, the optimal design is independent of the seismic load and is expected to be robust to the uncertainty in the earthquake records. Particle Swarm Optimization (PSO) as a well-explored optimization method in the control community has been selected as the appropriate algorithm for the optimization problem. Further details on PSO framework can be found in the literature.[37,38]

Once the optimal parameters have been obtained from the frequency domain analysis and its performance is assessed in the frequency domain, time history analyses are carried out to evaluate the TMDI-8, TMDI-9, and TTMDI-9

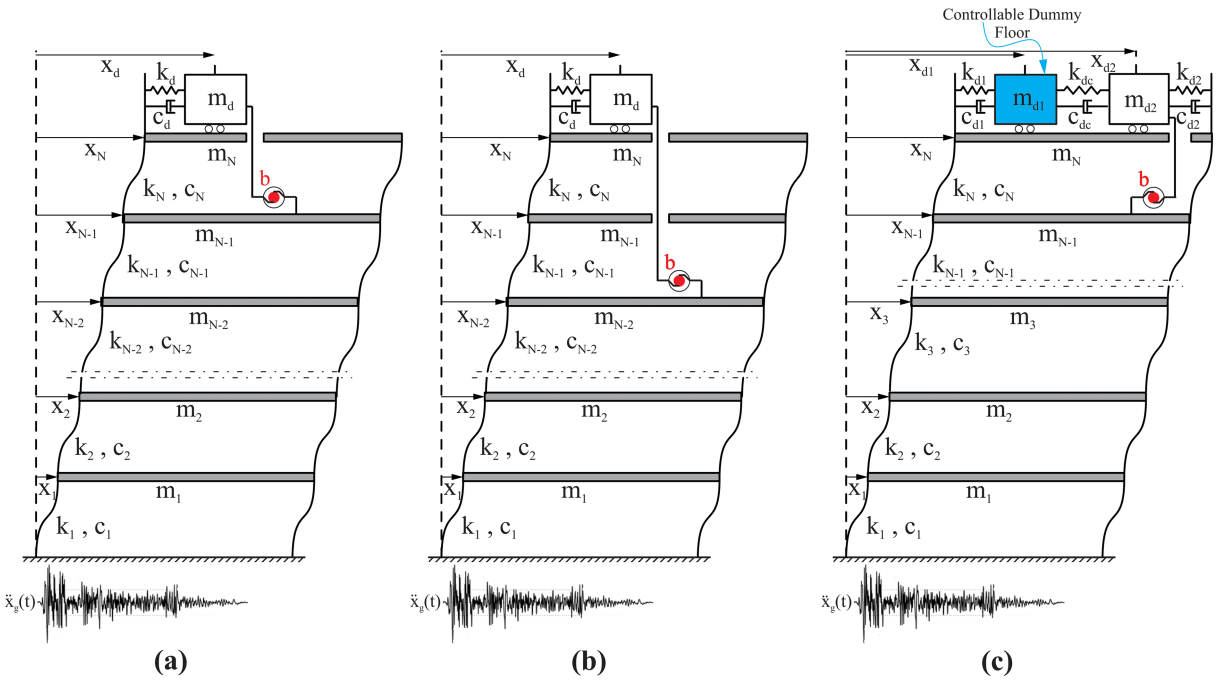

FIGURE 7 Schematic illustration for the N-story linear shear building with (a) TMDI-9, (b) TMDI-8, and (c) the proposed TTMDI-9

TABLE 2 Optimization variable definitions and variable ranges

	Model name		
	TMDI	**TTMDI**	
Preselected variables	$\beta = \frac{b}{M}$ $\mu = \frac{m_d}{M}$	$\beta = \frac{b}{M}$	$TMR(\mu) = \mu_1 + \mu_2 = \frac{m_{d1}}{M} + \frac{m_{d2}}{M}$
Preselected variable range	β = [0.05, 0.3, 1] TMR (μ) = 0.01	β = [0.05, 0.3, 1] TMR (μ) = $\mu_1 + \mu_2$ = 0.01	
Design variables	$f_d = \frac{\omega_d}{\omega_{1s}} = \frac{\sqrt{\frac{k_d}{m_d}}}{\omega_{1s}}$	$f_{d1} = \frac{\omega_{d1}}{\omega_{1s}} = \frac{\sqrt{\frac{k_{d1}}{m_{d1}+b}}}{\omega_{1s}}$	$\zeta_{d1} = \frac{c_{d1}}{2(m_{d1}+b)\omega_{d1}}$
		$f_{d2} = \frac{\omega_{d2}}{\omega_{1s}} = \frac{\sqrt{\frac{k_{d2}}{m_{d2}+b}}}{\omega_{1s}}$	$\zeta_{d2} = \frac{c_{d2}}{2(m_{d2}+b)\omega_{d2}}$
	$\zeta_d = \frac{c_d}{2m_d\omega_d}$	$f_{dc} = \frac{\omega_{dc}}{\omega_{1s}} = \frac{\sqrt{\frac{k_{dc}}{\overline{m}+b}}}{\omega_{1s}}$	$\zeta_{dc} = \frac{c_{dc}}{2(\overline{m}+b)\omega_{dc}}$
		$RMR = \frac{\mu_1}{\mu_2} = \frac{m_{d1}}{m_{d2}}$	
Design variable range	f_d = [0.0001 2] ζ_d = [0 2]	$f_{d1} = f_{d2}$ = [0.00001 2] $\zeta_{d1} = \zeta_{d2}$ = [0 2] RMR = [0.05 20]	

performance in the time domain, as further elaborated in Section 4. To this end, three sets of seven benchmark natural ground motions of far- and near-field earthquakes with forward directivity (FD) and fling step (FS) characteristics have been employed to take the uncertainty in the frequency content of earthquake records into account. A near-field record with FS is a ground motion that exhibits a permanent displacement in the displacement time history that is caused by the rupture of ground due to seismic activity.[39,41] On the other hand, forward directivity records are ground motions that present a double-sided dominant velocity pulse when the fault rupture propagates towards the site with a velocity equivalent to the shear wave velocity.[39,41] Near-field records are less subject to soil filtration due to their short distance to the epicenter and usually have a wider frequency content. Also, earthquakes with different characteristics can excite different modes of the structure and provide a more robust analysis of the performance of the proposed device. The records and relevant information are shown in Table 3, which are benchmark ground motions used in the literature.[19,39,40]

The evaluation of the damper efficiency in the time domain is based on two well-appreciated Engineering Demand Parameters (EDPs): the average of maximum story drift and the average of maximum absolute acceleration of the stories among the seven records of each set.

3 | OPTIMUM DESIGN OF THE CONTROL DEVICES

As mentioned previously, the optimum designs of TMDIs and TTMDI are determined using the PSO algorithm for the 10-story benchmark buildings with 2% inherent damping ratio. The optimum values of these variables are determined for 1% mass ratios and three different inertance ratios, 0.05, 0.3, and 1, representing low, medium, and high inertance ratio, respectively. Furthermore, the subset of model parameters that are preselected and necessary to characterize the design problem are organized in the vector $\boldsymbol{\varphi}$, which encompasses all information on the primary building, such as the number of stories, inherent damping ratio, and the damper mass ratio. On the other hand, the subset of model parameters that are selected as design variables, i.e., frequency and damping ratios of the TMDI, are organized in the vector of $\boldsymbol{\theta}$. Consequently, the optimum values of design variables $\boldsymbol{\theta}_{opt}$ is sought by means of the solution of the Equation (7), where $D_{\boldsymbol{\theta}}$ defines the search domain for design variables $\boldsymbol{\theta}$. The optimum design parameters for each device are summarized in Table 4 for different preselected inertance ratios. The last column in Table 4 presents the evaluation criterion of the damper performance, defined by Equation (8), i.e. the ratio of the largest singular value of the controlled to uncontrolled transfer function as a measure of the damper efficiency in the frequency domain.

$$\boldsymbol{\theta}_{opt}(\boldsymbol{\varphi}) = \underset{\boldsymbol{\theta} \in D_{\boldsymbol{\theta}}}{\operatorname{argmin}} \|\mathbf{G}(\boldsymbol{\theta}, \boldsymbol{\varphi}, s)\|_{\infty}, \tag{7}$$

TABLE 3 Seismic record information used in this study[19,39,40]

No	Year	Earthquake	Station	Com	Source	PGA (g)	PGV (cm/s)	PGD (cm)	Fling disp (cm)
(a) Far-field records									
1	1952	Kern County	Taft	111	1	0.18	17.50	8.79	—
2	1979	Imperial Valley	Calexico	225	1	0.27	21.24	9.03	—
3	1989	Loma Prieta	Presidio	00	1	0.10	12.91	4.32	—
4	1994	Northridge	Century CCC	90	2	0.26	21.19	7.85	—
5	1994	Northridge	Moorpark	180	2	0.29	20.97	5.48	—
6	1994	Northridge	Montebello	206	1	0.18	9.41	1.51	—
7	1971	San Fernando	Castaic	291	1	0.27	25.90	4.87	—
(b) Near-field records with forward directivity									
8	1992	Cape Mendocino	Petrolia	90	1	0.66	90.16	28.89	—
9	1994	Northridge	Olive View	360	1	0.84	130.37	31.72	—
10	1992	Erzincan	Erzincan	EW	1	0.50	64.32	21.93	—
11	2004	Parkfield	Fault Zone 1	FN	5	0.50	64.15	12.64	—
12	1984	Morgan Hill	Anderson Dam	340	2	0.29	28.00	12.19	—
13	1987	Superstition Hills	Parachute Test Site	315	1	0.45	112.00	52.46	—
14	1979	Imperial-Valley	Brawley Airport	225	1	0.16	35.85	22.39	—
(c) Near-field records with fling-step									
15	1999	Kocaeli	Yarimca (YPT)	EW	3	0.23	88.83	184.84	145.79
16	1999	Chi-Chi	TCU052	NS	4	0.44	216.00	709.09	697.12
17	1999	Chi-Chi	TCU068	EW	4	0.50	277.56	715.82	601.84
18	1999	Chi-Chi	TCU074	EW	4	0.59	68.90	193.22	174.56
19	1999	Chi-Chi	TCU084	EW	4	0.98	140.43	204.59	161.82
20	1999	Chi-Chi	TCU102	EW	4	0.29	84.52	153.88	73.66
21	1999	Chi-Chi	TCU128	EW	4	0.14	59.42	91.05	49.88

TABLE 4 Optimal parameters for different control devices based on minimizing the H_∞ norm of story drift

	Preselected parameters		Optimum parameters							Added mass		Performance criterion
Models	TMR	β	f_{d1}	ζ_{d1}	f_{d2}	ζ_{d2}	f_{dc}	ζ_{dc}	RMR	μ1	μ2	JF
TMDI-8	0.01	0.05	1.007	0.055	-					0.01	-	0.444
		0.3	1.117	0.071								0.437
		1	1.692	0.434								0.384
TMDI-9	0.01	0.05	1	0.045	-					0.01	-	0.498
		0.3	1.056	0.036								0.594
		1	1.258	0.063								0.589
TTMDI-9	0.01	0.05	0.896	0	1.13	0	0.489	0.435	0.05	0.0095	0.0005	0.293
		0.3	0.968	0	1.195	0.027	0.114	1.578	0.05	0.0095	0.0005	0.291
		1	0.006	0.647	2	2	1.351	0.114	0.05	0.0095	0.0005	0.301

$$JF\left(\boldsymbol{\theta}_{opt},\boldsymbol{\varphi}\right)=\frac{\left\|\mathbf{G}\left(\boldsymbol{\theta}_{opt},\boldsymbol{\varphi},s\right)\right\|_{\infty}}{\left\|\widehat{\mathbf{G}}\left(\boldsymbol{\varphi},s\right)\right\|_{\infty}}. \tag{8}$$

Table 4 shows that the TTMDI-9 has resulted in a better performance with respect to both TMDI-8 and TMDI-9 in the frequency domain; i.e., the TTMDI-9 has successfully reduced the uncontrolled response to approximately 30%. Moreover, the TTMDI-9 has been able to beat the TMDI-8 and TMDI-9 by an average of 30% and 47%, respectively. In other words, the TTMDI-9 has even outperformed the TMDI-8 significantly, without creating architectural problems from a practical point of view.

Comparison of the performance of TMDI-8, TMDI-9, and TTMDI-9 in the last column of Table 4 reveals the paradoxical effect of inertance. Although in studies on single-degree-of-freedom (SDOF) models of grounded TMDI (GTMDI), increasing the inertance has improved the responses significantly,[23,24,42,43] the same monotonous effect cannot be expected for multi-degree-of-freedom (MDOF) structures equipped with rooftop TMDI.[23,24,28,42] In fact, it has been shown in previous studies that the introduction of inertance in the TMDI is accompanied by two opposite characteristics of negative stiffness and mass amplification effects.[18,23] For a rooftop TMDI, the smaller the Δφ (i.e., moving the second terminal of the inerter towards the roof), the greater the negative stiffness effect, and the higher Δφ (i.e., moving the second terminal of the inerter towards the ground), the greater the mass amplification effects.[23,24] Negative stiffness reduces the efficiency of the rooftop TMDI, while mass amplification enhances its performance. Furthermore, increasing the inertance ratio (β) can exacerbate both the negative stiffness and mass amplification effects.[23,24] Therefore, in the range of the Δφ that negative stiffness effect dominates the mass amplification, an increase in inertance will have a negative effect, while in the range of Δφ where mass amplification dominates the negative stiffness effects, increasing inertance is expected to have a positive effect on the TMDI performance. This is an example of the interaction effect of TMDI inertial parameters, which has been reported in previous studies and makes the evaluation of damper performance with increasing inertance dependent on mass ratio values, and especially the Δφ parameter.[23,24]

In Table 4, this dual effect of inertance on damping performance is well illustrated by comparing the behavior of TMDI-9 (with smaller Δφ and near-roof inerter connection) and TMDI-8 (with larger Δφ and lower floor connection). In other words, in TMDI-9, the Δφ is probably in the range that the negative stiffness dominates the mass amplification and, therefore, increasing inertance has reduced the performance of the TMDI. On the other hand, for TMDI-8, the Δφ must be in the range that the mass amplification outweighs the negative stiffness and, therefore, increasing inertance has enhanced the performance of the TMDI-8. For the TTMDI-9, the asymmetric mass distribution has potentially resulted in a higher Δφ (Figure 8), and therefore, it has shown the biggest reduction in responses, while not being sensitive to the variation of inertance. This matches well with the literature,[23] where it has been shown that for TMDIs with small mass ratio, adding an extremely small inertance will significantly improve the response initially up to a certain

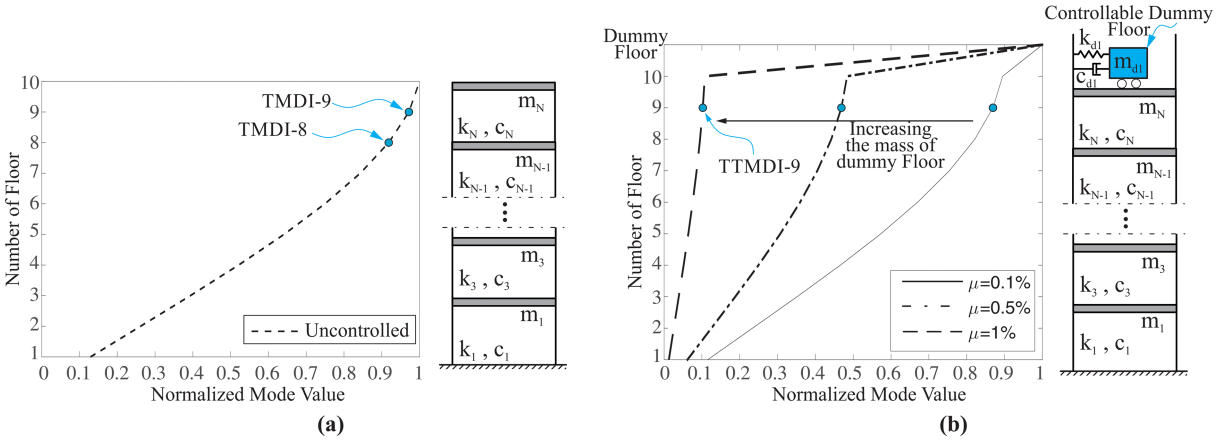

FIGURE 8 The normalized first modal shape for the (a) uncontrolled structure and (b) structure with an added controllable dummy floor

limit, after which it reaches an asymptote. Presumably, the same applies to the TTMDI-9 with an extremely small, attached mass to the inerter.

It is noteworthy that since the RMR was selected as a design variable for the TTMDI-9 control device, the optimization has resulted in a counterintuitive "biased" mass distribution, i.e., RMR = 0.05. In other words, the smaller mass (m_{d2}) has reached the lower bound of the design variables. Therefore, equal added masses do not necessarily yield better control results with the justification provided herein. As mentioned earlier, the inerter location parameter, $\Delta\varphi$, plays an important role in the performance of inerter-based tuned mass dampers (TMDI-based), and local modification of the modal shape at the upper floors (increasing $\Delta\varphi$) has proven to enhance the performance of TMDIs.[29,30]

Figure 8 shows the effect of adding the controllable dummy floor on the first mode shape of the host building along with the modal shape values at the position of the second terminal of the inerter. If a TMDI is added to Figure 8a/b, the building controlled by TMDI/TTMDI will be obtained, respectively. In Figure 8b, μ represents the mass ratio of the controllable dummy floor. The locations of the second terminal of the inerter are shown with blue dots on the modal shape, which clearly show that by increasing the controllable dummy floor mass, $\Delta\varphi$ increases; in other words, as more percentage of the mass is allocated to the controllable dummy floor, the local change in modal shape of the upper floors will be more significant, which is more desirable in terms of enhancing the TMDI performance. Previous studies[23,24] have also shown that the inerter is more effective in in reducing the structural response when the mass ratio is small. Therefore, the tendency of the optimization process to asymmetrically divide the total presumed mass into a larger controllable dummy floor mass and a smaller TMDI mass may be due to the increased local changes in the mode shape and higher inerter efficiency with less mass for the TMDI, respectively. Although, there can be other possible effective configurations (e.g., assigning all the mass to one of the masses and the remainder being a combination of spring/damper/inerter), a comprehensive parametric study is needed if any comparison is to be made with the proposed TTMDI configuration and is, therefore, excluded herein. The main purpose of this study was to overcome the practical challenges of lowering the second terminal of inerter in rooftop TMDIs to enhance its performance.

Figures 9a–c shows the singular value of the story drift transfer function for the building with optimal TMDI-8, TMDI-9, and TTMDI-9 devices for 1% preselected mass ratios and three different inertance ratios of 0.05, 0.3, and 1, respectively. The results for the uncontrolled structure are also presented for comparison purposes. Figure 9d–f similarly shows the diagrams for the absolute story acceleration transfer function. Figure 9 indicates that for the 1% preselected mass ratio, TTMDI-9 has successfully mitigated the response and outperformed both TMDI-8 and TMDI-9 configurations in terms of drift and absolute story acceleration for the first mode, except for the acceleration response

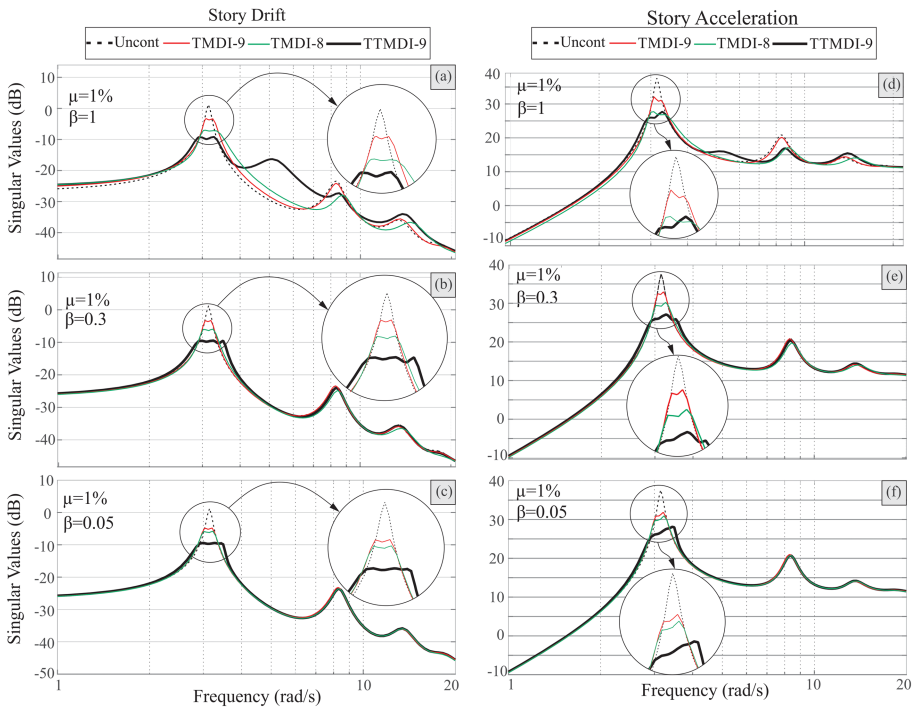

FIGURE 9 Frequency response of story drift and absolute acceleration for different cases

with $\beta = 1$. For this special case, the TMDI-8 and TTMDI-9 configurations have almost the same performance and have outperformed the TMDI-9. In addition, the reduction of singular value for the second mode is also of the same order for TMDI-8 and TTMDI-9 and better than the TMDI-9, especially for high inertance ratio.

Furthermore, as shown in Figure 9 and Table 4, increasing the inertance ratio (β) has non-monotonous effect on the frequency response of the controlled building in the first mode. To the contrary, the effect of increasing inertance is monotonous in higher modes, and the frequency response decreases in the TMDI-8 and TTMDI-9 for large inertance ratio. This can be presumably attributed to the fact that mass amplification has become predominant due the larger curvature and higher Δφ of the modal shape values between the inerter terminal locations in these higher modes. Since the modal shape curvature and, consequently, the Δφ at the two inerter levels are typically greater in the higher modes than that for the fundamental mode, the modal shape modification has little effect on improving the response in the higher modes, especially between TMDI-8 and TTMDI-9.

4 | PERFORMANCE ASSESSMENT IN TIME DOMAIN

The performance of the 10-story building with 2% inherent damping ratio is examined under three groups of seven natural earthquakes with far- and near-field records with FD and FS characteristics to evaluate the efficiency and robustness of the optimum designed dampers in the time domain. The performance criteria in the time domain are peak story drift in the controlled building normalized by the corresponding story drift in the uncontrolled building (*JT1*) and peak absolute story acceleration in the controlled building normalized by the corresponding acceleration in the uncontrolled building (*JT2*) defined based on Equations (9) and (10), respectively, where f = floor number, 1, ..., 10; q = earthquake number: 1, ..., 21, and t = time, $0 \le t \le T_q$, where T_q is the duration of earthquake q. In Equations (9) and (10), d and a represent the drift and absolute acceleration of the controlled structure, respectively, while $\widehat{d}$ and $\widehat{a}$ represent those of the uncontrolled structure, respectively. In both equations, $|.|$ represents the absolute value. So $\max_{t,f}\left|d_f(t,q)\right|$ represents the maximum of the absolute value of drift (during the duration of earthquake q) for all the floors of the building. These performance criteria are a good measure for structural failure and occupancy comfort level.

$$JT1(q) = \frac{\max_{t,f}\left|d_f(t,q)\right|}{\max_{t,f}\left|\widehat{d}_f(t,q)\right|}, \tag{9}$$

$$JT2(q) = \frac{\max_{t,f}\left|a_f(t,q)\right|}{\max_{t,f}\left|\widehat{a}_f(t,q)\right|}. \tag{10}$$

Tables 5 and 6 present the *JT1* and *JT2* criterion for the 10-story building with 2% inherent damping ratio, 1% mass ratio and all three different studied inertance ratios for every single natural earthquake of the three different groups. As previously mentioned, the optimization has been performed based on the minimization of inter-story drift, and the acceleration criterion has been used to show the implicit effect of single value optimum design of control devices on other important EDPs. The lowest values of the *JT1* are 0.7, 0.94 and 0.68 under far- and near-field records with FD and FS characteristics, respectively, which shows the best performance under near-field records with FS and far-field records, and an acceptable performance under near-field records with FD. Table 5 indicates that the TTMDI-9 has a superior performance with respect to its equivalent counterpart, i.e., TMDI-9, under far-field records, with an average of 7–9% improvement in story drift response for all inertance ratios. However, for the near field records with FD and FS, except for $\beta = 1$ where there is about 9% reduction in response, the TTMDI-9 and TMDI-9 perform almost similarly, with the former performing slightly better (maximum average of 3%). Therefore, the TTMDI-9 has been able to show enhanced efficiency, as well as robustness compared to the TMDI-9. In addition, the proposed damper has a similar performance to that of TMDI-8 for all record types without creating any additional architectural interference.

On the other hand, Table 6 shows that the lowest value of *JT2* index are 0.74, 0.75, and 0.67 under far- and near-field records with FD and FS characteristics, respectively, which similarly shows the best performance under near-field records with FS records and an acceptable performance under far- and near-field records with FD. Although the optimization objective function was not related to the minimization of story acceleration, the *JT2* value shows a comparable

TABLE 5 Normalized maximum story drift, JT1

β	0.05			0.3			1		
Models / Earthquake Number	TTMDI-9	TMDI-9	TMDI-8	TTMDI-9	TMDI-9	TMDI-8	TTMDI-9	TMDI-9	TMDI-8
Far-field records									
1	**0.94**	0.98	0.97	**0.94**	1.00	0.97	**0.93**	0.99	**0.93**
2	**0.70**	0.88	0.84	**0.71**	0.95	0.84	**0.70**	0.95	0.82
3	**0.95**	0.99	0.99	**0.95**	1.00	0.98	0.93	1.00	**0.91**
4	**0.94**	0.97	0.96	**0.93**	0.97	0.95	0.90	0.97	**0.89**
5	**0.92**	0.97	0.97	**0.92**	0.98	0.97	**0.92**	0.99	0.94
6	**0.81**	0.93	0.90	**0.81**	0.95	0.86	**0.85**	0.92	0.91
7	**1.00**	**1.00**	1.01	**1.00**	**1.00**	1.03	**1.01**	**1.01**	1.07
Near-field records with forward directivity									
8	**0.97**	0.99	0.99	**0.97**	1.00	0.99	**0.96**	1.00	0.98
9	**0.95**	0.99	0.99	**0.95**	0.99	1.00	**0.96**	1.00	0.98
10	**0.97**	0.99	1.00	**0.98**	1.00	1.01	**1.00**	1.01	1.04
11	**1.00**	1.00	**1.00**	**0.99**	1.00	**0.99**	0.97	1.00	**0.95**
12	**1.00**	1.02	1.01	1.00	1.02	**0.99**	0.95	1.02	**0.94**
13	0.98	**0.97**	0.98	**0.97**	**0.97**	0.98	0.97	0.97	**0.96**
14	**0.99**	1.01	1.01	**0.99**	1.01	1.00	**0.98**	1.01	**0.98**
Near-field records with fling step									
15	**0.95**	0.97	0.96	**0.95**	0.98	**0.95**	**0.94**	0.97	**0.94**
16	**0.95**	0.99	0.99	**0.95**	1.00	0.99	**0.95**	1.00	0.97
17	**0.91**	1.00	0.98	**0.91**	1.01	0.97	**0.91**	1.00	0.93
18	**0.99**	1.00	1.00	0.99	1.00	**0.97**	0.93	1.00	**0.86**
19	**0.90**	0.96	0.96	**0.90**	0.98	0.96	**0.90**	0.98	0.93
20	**0.95**	0.99	0.99	**0.95**	1.00	0.99	**0.95**	1.00	0.99
21	**0.69**	0.90	0.85	**0.68**	0.95	0.83	**0.68**	0.93	0.73

Note: Bold text shows the best performance.

performance under all record types, especially near-field with FS for high values of inertance ($\beta = 1$). Generally, for *JT2*, the TTMDI-9 outperformed its counterpart TMDI configurations, i.e., TMDI-9, in all cases. For *JT2*, the TMDI-8 performed slightly better (approximately 5–6%) when comparing the average of response; however, there is no complete superiority for any specific configuration, as shown in Table 6.

It should be noted that Tables 5 and 6 provide only a general overview of the performance of the control devices and important information may be excluded in the process. Therefore, the distribution of the performance indices along the building height for each earthquake as well as for the average of indices is depicted next. For the sake of brevity, results for the worst case in the frequency domain, i.e., $\beta = 1$, are presented in Figures 10–12 and Figures 13–15 for *JT1* and *JT2*, respectively. In Figures 10–15, the vertical and the horizontal axes represent the story number and the studied criteria, i.e., *JT1* and *JT2*. Additionally, the performance of the uncontrolled building along with those of the three different control configurations, i.e., TTMDI-9, TMDI-8, and TMDI-9, are presented for each set of records separately, as well as for the average of the records in each case with red, blue, black, and green colors, respectively. The mean performance of each configuration for each story is also presented and compared in part (e) of the figures. The performance of each story in all graphs is normalized to the maximum uncontrolled value of the whole height of the building under each single record. Moreover, the orange dashed vertical line that passes through a value of 1 shows the uncontrolled performance in each graph.

Figures 10–12 demonstrate and compare the peak story drifts along the height under far- and near-field records with FD and FS, respectively. Figure 10 shows that in most cases, the control devices have been successful in suppressing the

TABLE 6 Normalized maximum story acceleration, JT2

β	0.05			0.3			1		
Models / Earthquake Number	TTMDI-9	TMDI-9	TMDI-8	TTMDI-9	TMDI-9	TMDI-8	TTMDI-9	TMDI-9	TMDI-8
Far-field records									
1	0.94	0.95	**0.93**	0.91	0.93	**0.84**	0.79	0.87	**0.66**
2	**0.97**	0.98	**0.97**	0.96	0.97	**0.91**	0.85	0.93	**0.75**
3	**0.96**	**0.96**	0.97	0.95	0.95	**0.91**	0.86	0.93	**0.74**
4	0.98	**0.96**	0.97	0.97	**0.95**	0.98	0.98	**0.95**	0.98
5	**0.94**	0.99	0.97	0.93	0.99	**0.90**	**0.87**	0.94	0.88
6	1.00	**0.99**	1.02	1.02	**1.01**	1.08	1.10	**1.04**	1.19
7	0.99	**0.98**	**0.98**	0.97	0.97	**0.91**	0.86	0.92	**0.80**
Near-field with forward directivity records									
8	**0.98**	**0.98**	**0.98**	0.97	0.97	**0.93**	0.88	0.94	**0.81**
9	**0.98**	**0.98**	0.99	0.96	0.96	**0.91**	0.87	0.90	**0.82**
10	**0.94**	0.97	0.96	0.94	0.97	**0.92**	0.89	0.95	**0.81**
11	0.99	0.99	**0.98**	0.98	0.98	**0.93**	0.90	0.95	**0.83**
12	0.99	**0.97**	**0.97**	0.96	0.94	**0.85**	0.76	0.87	**0.75**
13	**0.95**	0.97	**0.95**	0.93	0.96	**0.90**	0.89	0.93	**0.84**
14	**0.94**	0.98	0.96	0.93	0.97	**0.91**	0.88	0.94	**0.80**
Near-field with fling step records									
15	**0.83**	0.93	0.90	**0.83**	0.95	0.84	0.72	0.92	**0.70**
16	**0.95**	0.98	0.96	0.93	0.98	**0.92**	0.91	0.96	**0.85**
17	**0.97**	0.98	0.98	0.96	0.97	**0.93**	0.91	0.95	**0.88**
18	0.99	0.98	**0.97**	0.97	0.97	**0.89**	0.84	0.93	**0.66**
19	**0.92**	0.96	0.94	**0.90**	0.96	**0.90**	0.84	0.93	**0.79**
20	**0.95**	0.97	0.97	0.94	0.97	**0.92**	0.89	0.95	**0.79**
21	**0.78**	0.86	0.83	**0.76**	0.87	0.77	0.73	0.83	**0.67**

Note: Bold text shows the best performance.

structural drift for far-field records. The only configuration that crossed the uncontrolled threshold by about 8% is TMDI-8 (Figure 10c). Comparing the mean performance of uncontrolled and controlled buildings shows that the TTMDI-9 has the best performance among the different control devices over the height of the building and has significant advantage over the TMDI-9 and TMDI-8 configurations on lower and upper stories. In addition, it has overcome the undesirable control performance that the TMDI configurations have on the upper stories, an important issue that could remain hidden if the maximum responses were only compared. To the contrary, the mean story drift in the TTMDI-9 configuration never exceeds the mean uncontrolled response, which is a great achievement in terms of robustness.

In Figures 11 and 12, a similar assessment has been performed for near-field records with FD and FS, respectively, which shows that the TTMDI-9 has outperformed both TMDI-9 and TMDI-8 configurations under both near-field records, especially in the two upper stories, where the TMDI configurations show a poor performance with respect to the uncontrolled state. It is also evident that for both TMDI configurations under near-field records with FD, the responses may cross the uncontrolled threshold at the base, which is a significant robustness concern and could compromise the stability of the building. Comparison of Figures 10e, 11e, and 12e show that the TTMDI-9 has outperformed the studied TMDI configurations under all three different earthquake groups and the best performance is achieved under far-field records.

To evaluate the effect of single-objective optimization of the studied configurations and assess its effects on other substantial EDPs, the maximum absolute story accelerations of the uncontrolled and controlled buildings along the

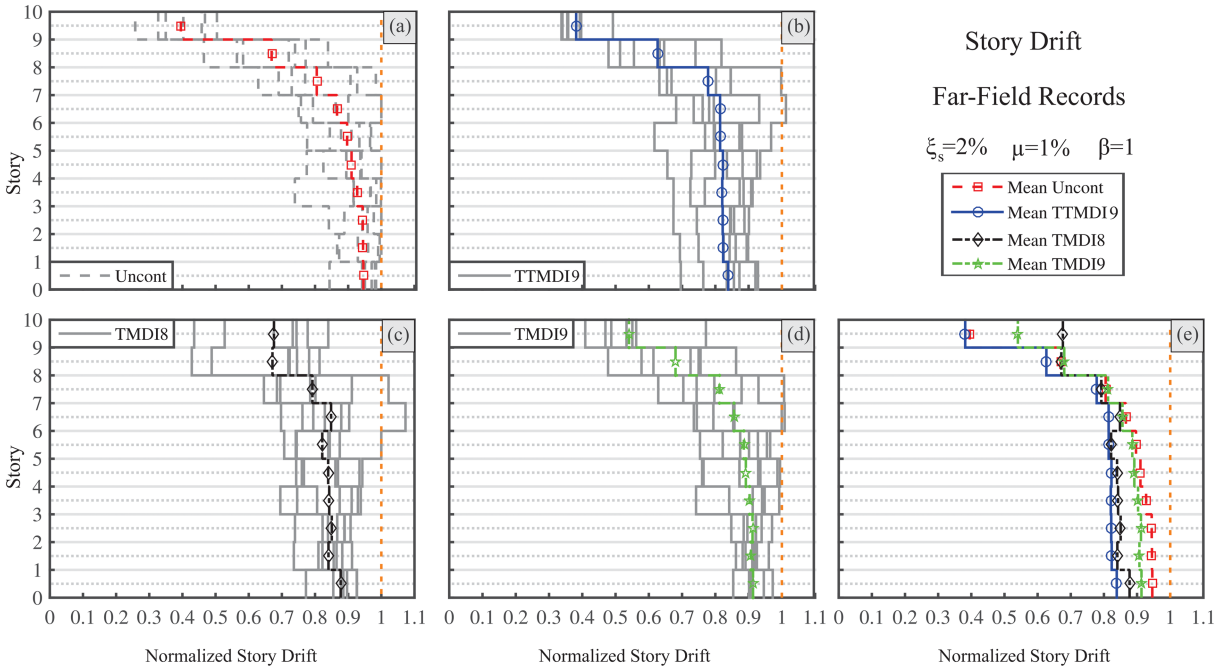

FIGURE 10 Maximum normalized story drift under far-field records

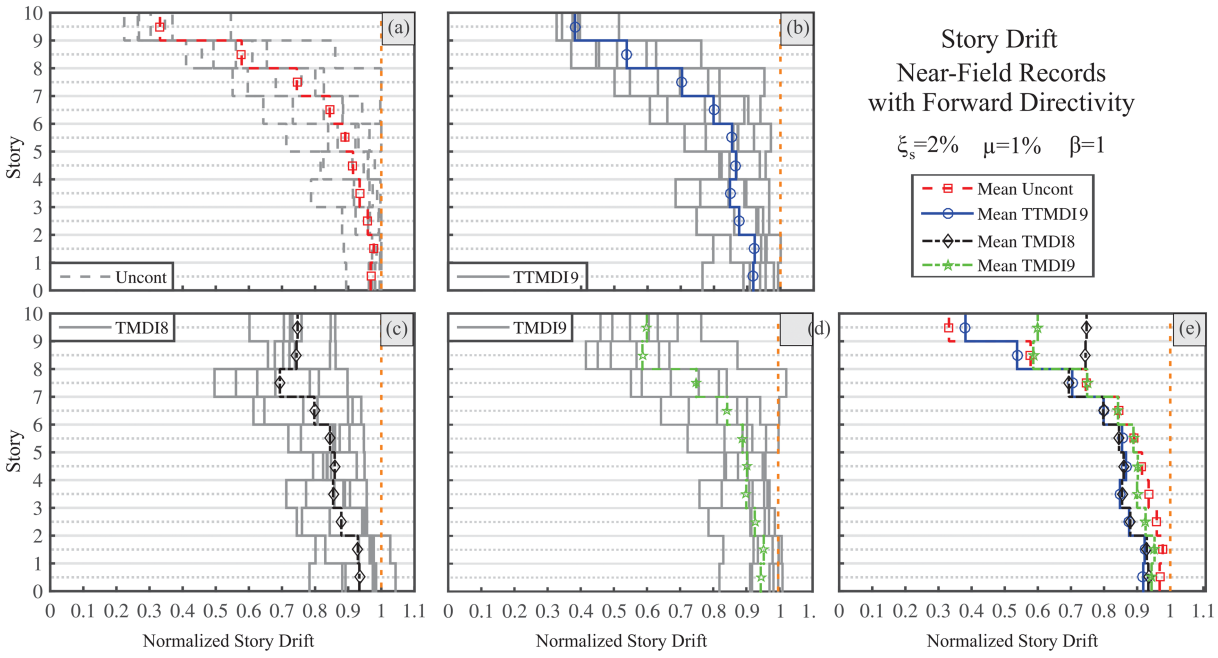

FIGURE 11 Maximum normalized story drift under near-field records with FD

height are displayed in Figures 13–15. Figure 13 shows the maximum absolute story accelerations of the uncontrolled and controlled buildings under far-field records. In general, all three TMDIs and TTMDI configuration have exceeded the uncontrolled threshold for one single record under far-field excitation, while the story acceleration is always below the uncontrolled threshold under near-field records with FD and FS, as shown in Figures 14 and 15. The exceedance of the story drift from the uncontrolled state under far-field records is more profound for TMDI-8 and can reach up to 20%, which implicates robustness concerns. Nevertheless, this is only observed under one single record and cannot be noticed for other records. In addition, in almost all cases, the TMDI-8 has the best performance in terms of acceleration response and is closely followed by the TTMDI-9. In other words, a close performance with about under 5% difference

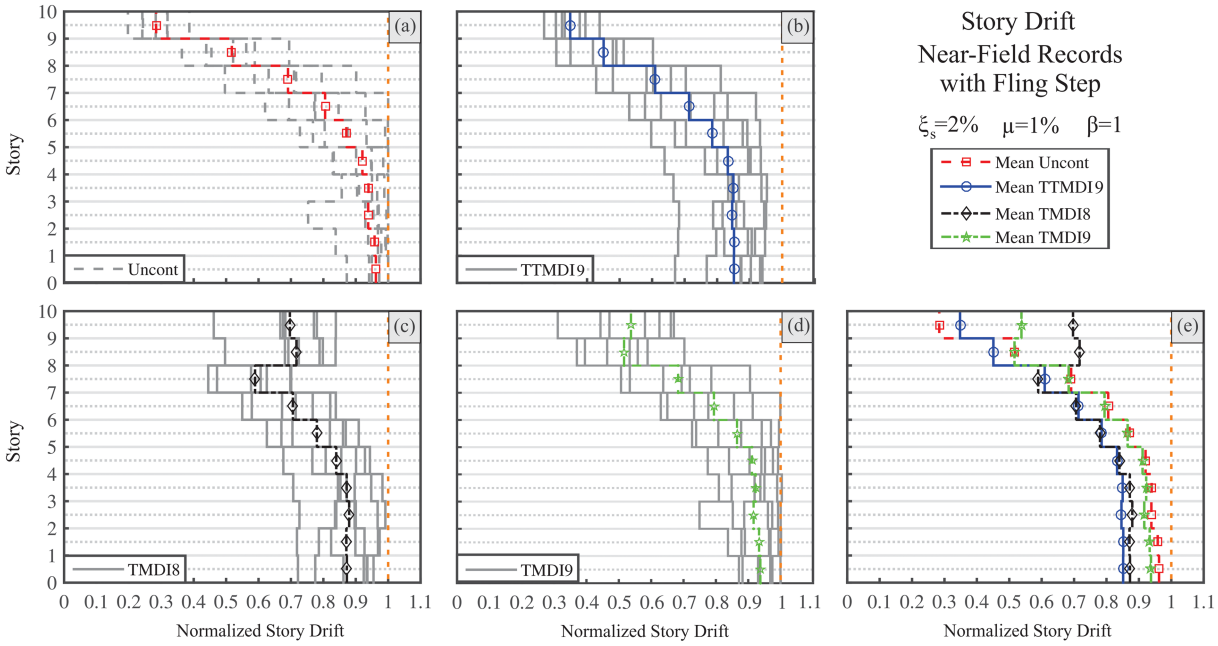

FIGURE 12 Maximum normalized story drift under near-field records with FS

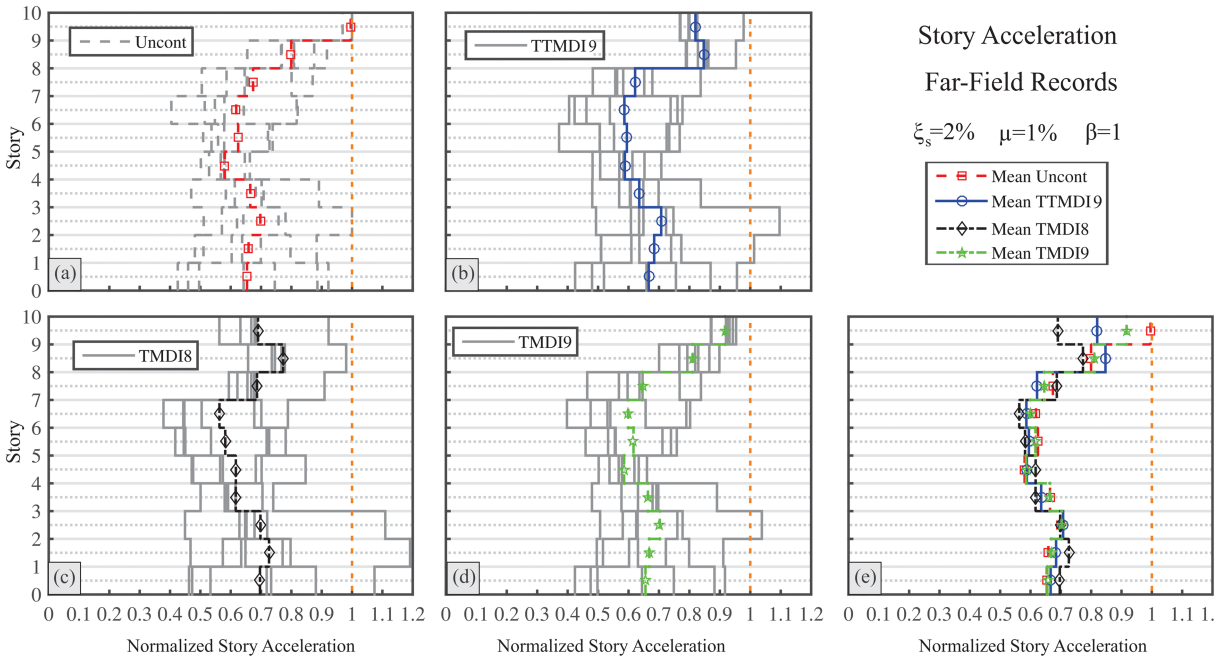

FIGURE 13 Maximum normalized story acceleration under far-field records

in results for TMDI-8 and TTMDI-9 is observed. In Figures 13e–15e, it is evident that the difference between the performances of all three configurations is concentrated in the upper two stories. Additionally, the maximum acceleration reductions of all configurations under all record groups are almost the same and closely under 10% and above 20% for TMDI-9 and TMDI-8, respectively, while about 15% is observed for TTMDI-9. Moreover, comparing the presented results for drift reduction performance (Figures 9e–11e) with their corresponding result for acceleration reduction (Figures 13e–15e) ascertains the better performance of all configurations in acceleration reduction.

Past research has shown that near-field records with FS excite the structures mainly in their fundamental mode, while near-field records with FD typically excite higher modes of vibration.[39,41] Therefore, it is expected that the

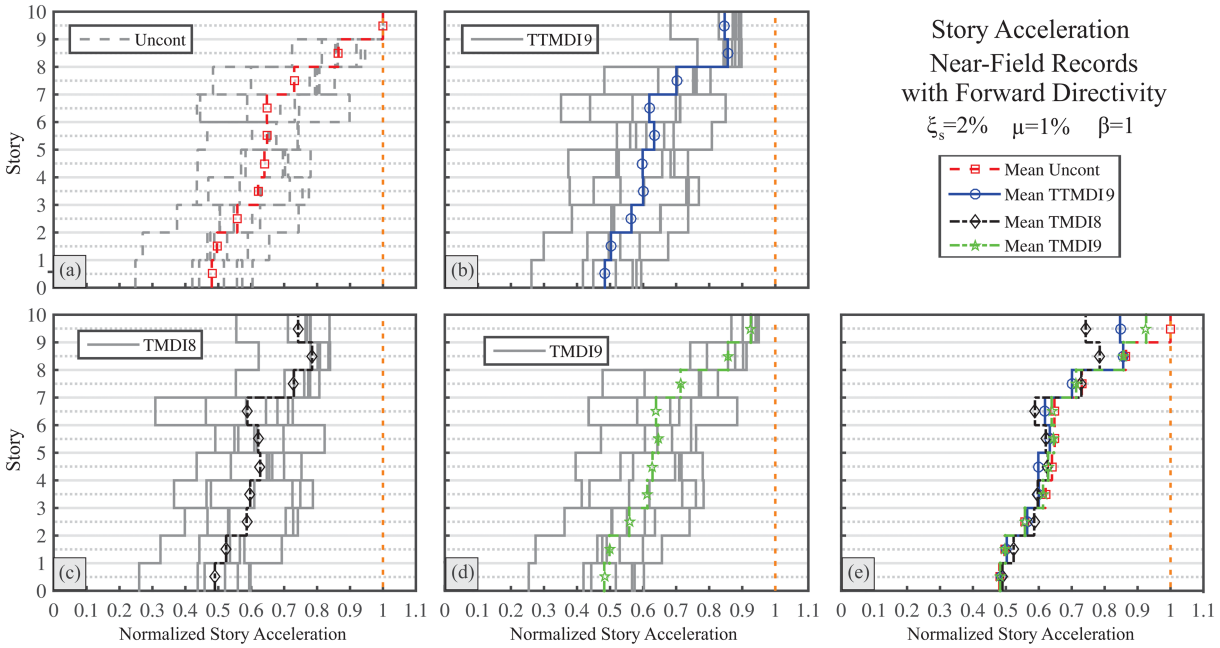

FIGURE 14 Maximum normalized story acceleration under near-field records with FD

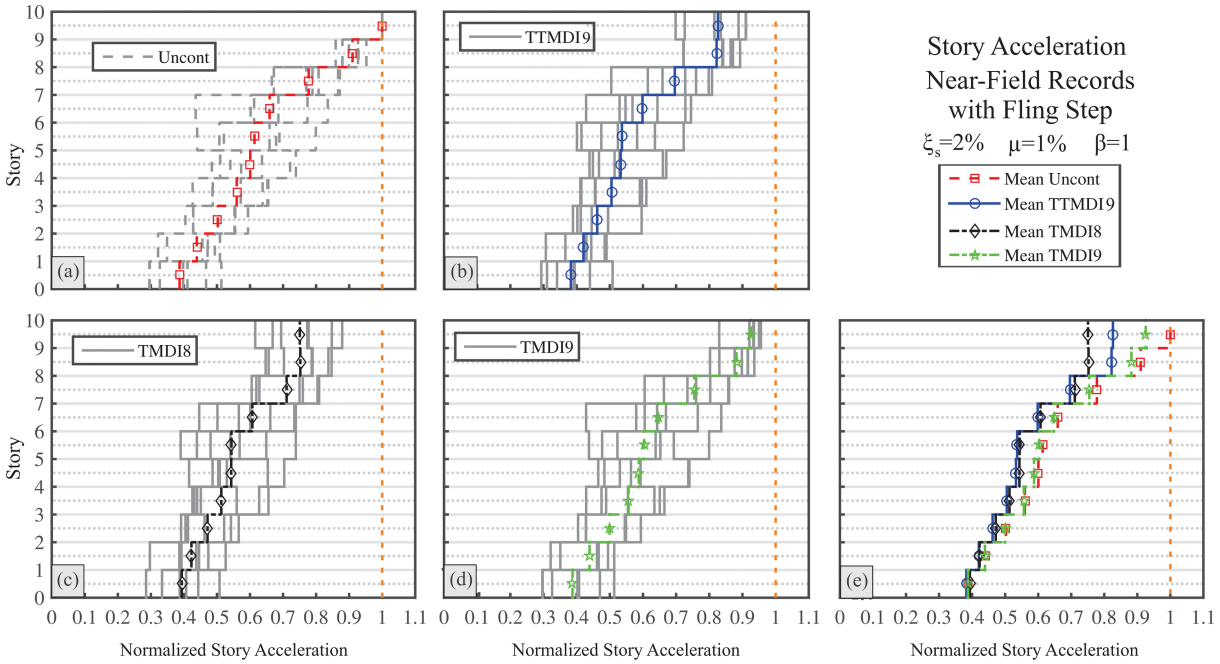

FIGURE 15 Maximum normalized story acceleration under near-field records with FS

difference between different devices in improving the drift in the time domain exhibits itself better under the records with FS. This is clearly visible in the response in the time domain in Figures 11 and 12 both in the average of record responses (part e), as well as under individual records (remaining parts of both figures; pay attention to the scattering of the responses). Figures 11 and 12 also show that similar to the frequency response domain responses (Figure 9), the performances of the TMDI-8 and TTMDI-9 are very close. The same could be observed from Table 5, where the lowest value of JT1 was observed for near-field records with FS characteristics. On the other hand, since near-field records with FD excite higher modes of vibration, it is expected that the absolute acceleration (which is a higher frequency type response) is more affected by these records for the high value of inertance ratio (β), as clearly observed in Figures 14

and 15. This also matches the observation in the frequency domain (Figure 9), where the effect of high inertance exhibits itself in the second mode. Therefore, in the time domain (Figures 14 and 15), the performance of TMDI-8 and TTMDI-9, and TMDI-9 and uncontrolled structure in terms of absolute story acceleration are expected to be similar.

5 | LIMITATIONS AND FUTURE STUDIES

The focus of the current study is to find a solution to the main problem of rooftop TMDI (i.e., the need of inerter to be connected to the lower stories) with the least structural and architectural interference. Our study shows that the proposed damper (TTMDI-9) indeed improves the performance of TMDI without the need to increase the distance between its two terminals. In other words, the TTMDI-9 overcomes the construction limitation of the TMDI-8, while providing the same level of response mitigation and improving the performance of its direct counterpart, i.e., TMDI-9. It should be noted that the total mass of the TMDI/TTMDI is another important parameter that affects its performance, and these conclusions for these specific configurations are valid for the 1% mass ratio. In general, the interactions between the parameters of the TMDI make it very difficult to predict its performance without analysis.[19,23–30,42] The added design parameters of the TTMDI makes the process even more difficult.

Furthermore, for comparison of the proposed device with TMD, one should recognize that the performance of TMD is characterized solely by its mass, while in the TMDI, mass ratio, inertance ratio, and the inerter location parameter ($\Delta\varphi$) play a significant role in its performance. While this increase in the number of parameters gives more flexibility to the design and allows for an improved response in certain range of $\Delta\varphi$ and β, at the same time, it complicates the process of optimization due to both direct and interactive effects of design parameters on the damper performance. In addition, the relationship between TMDI performance and its three design parameters is nonlinear. Therefore, any comparison of the performance of these control devices with TMD should be done in a comprehensive parametric study that includes a suitable and continuous range of parameters. In TTMDI, the number of controllable inertial parameters is even more, making the complexity and interaction effects more difficult compared to the TMDI. Therefore, comparison of the performance of TTMDI and TMD should be done in an in independent comprehensive parametric study and is excluded herein.

6 | SUMMARY AND CONCLUSION

In this study, a tandem tuned mass damper inerter (TTMDI) is proposed, in which the mass of a conventional tuned mass damper inerter (TMDI) is divided into two variable masses that are connected to each other using a spring and dashpot, and one of the masses is connected to an inerter device. The purpose of dividing the total mass of a rooftop TMDI is virtually increasing the distance between the two terminals of the inerter by allocating part of the mass to create a controllable dummy floor, which would result in a local change in the modal shape values, $\Delta\varphi$ (inerter location parameter), without interfering with architectural features in the lower stories. The proposed TTMDI is employed for the structural control of a benchmark 10-story linear shear building with 2% inherent damping ratio, and its efficiency and robustness are evaluated in both frequency and time domains. Results are presented for a preselected total mass ratio of 0.01 and three preselected inertance ratios of 0.05, 0.3 and 1. For the time-domain analysis, three sets of far-field and near-field records with forward directivity (FD) and fling step (FS) are considered, in which each set consisted of seven time history accelerations. The free parameters of the TTMDI (frequency and damping ratio of the two masses and their connecting spring and dashpot as well as their mass ratio) are optimized using particle swarm optimization algorithm (PSO) by minimizing the largest singular value of story drift transfer function. Results are also computed for two comparable rooftop TMDIs, i.e., TMDI-9 and TMDI-8 for comparison purposes, in which the second terminal of the inerter is connected to the 9th and 8th stories, respectively.

The frequency domain analyses show that the TTMDI-9 performs better than both TMDI-8 and TMDI-9, successfully reducing the response by an average of 30% and 47%, respectively. In other words, the TTMDI-9 has even outperformed the TMDI-8 significantly, without creating architectural problems form a practical point of view. Comparison of the performance of TMDI-8, TMDI-9, and TTMDI-9 reveals the paradoxical effect of inertance in MDOF structures due to the interaction effects between the total mass ratio, relative mass ratio, inertance ratio, and inerter location parameter. In addition, the optimization algorithm resulted in a counterintuitive "biased" mass distribution, where the majority of the total mass was allocated to the controllable dummy floor and an extremely small portion was

assigned to the mass that was connected to the inerter. Results showed that a larger mass for the controllable dummy floor that increases the local changes in the mode shape, combined with a smaller mass for the TMDI, warrants a better performance of the proposed device compared to the TMDI-8 and TMDI-9 dampers.

For the time domain, story drift and absolute story acceleration are selected as performance criteria, since they are closely related to both failures in structural and non-structural components. Results have been both presented as tabulated normalized maximum responses, as well as the normalized story drift and absolute acceleration distribution along the building height for the individual earthquakes and the corresponding average to each earthquake sets. Considering the maximum normalized story drift, the TTMDI-9 has shown 7–9% improvement for all inertance ratios with respect to its equivalent counterpart, i.e., TMDI-9, under far-field records, while for near-field record records, except for $\beta = 1$ where there is about 9% reduction in story drift, the TTMDI-9 and TMDI-9 perform almost similarly, with the former performing slightly better (maximum average of 3%). In addition, the proposed damper has a similar performance to that of TMDI-8 for all record types without creating any additional architectural interference. Comparing the average of story drifts along the height shows that the TTMDI-9 has the best performance among the different control devices and has significant advantage over the TMDI-9 and TMDI-8 configurations on lower and upper stories. In addition, it has overcome the undesirable control performance of the TMDI configurations have on the upper stories, an important issue that could remain hidden if the maximum responses were only compared.

The time-domain analyses for near-field records shows that for both TMDI configurations, the responses could cross the uncontrolled threshold at the base, which is a significant robustness concern and could compromise the stability of the building, while the TTMDI-9 configuration did not exhibit such results. Comparing the average of absolute acceleration along the heights reveals that generally the TTMDI-9 and TMDI-8 have almost similar performance, with the TMDI-8 showing about 5% better performance in acceleration reduction only in the two upper stories. However, for one of the far-field records, the TMDI-8 showed about 20% exceedance of the uncontrolled response threshold, which can be considered as a robustness concern. Therefore, although all configurations have successfully reduced the structural responses, the TTMDI-9 configuration has demonstrated the best and most reliable performance and does not create additional architectural interference problems like the TMDI-8 configuration. Additionally, due to many different load paths in this configuration compared to the TMDIs, it could be much reliable under any abruption of connecting stiffness or dampers, and splitting the mass could also be helpful from a practical construction point of view. Nevertheless, ensuring the last two advantages needs further studies.

AUTHOR CONTRIBUTIONS

Maziar Fahimi Farzam was responsible for writing the first draft and revised manuscript, as well as conceptualization, software, methodology, formal analysis, validation, and data visualization. Himan Hojat Jalali contributed to the conceptualization, methodology, visualization, writing the original draft, and review and editing of the revised manuscript.

DATA AVAILABILITY STATEMENT

Data supporting the findings of this study are available from the corresponding author upon request.

ORCID

Maziar Fahimi Farzam https://orcid.org/0000-0001-9635-8186
Himan Hojat Jalali https://orcid.org/0000-0002-0075-9725

REFERENCES

1. Elias S, Matsagar V. Research developments in vibration control of structures using passive tuned mass dampers. *Annu Rev Control*. 2017;44:129-156. doi:10.1016/j.arcontrol.2017.09.015
2. Salvi J, Rizzi E. Optimum tuning of tuned mass dampers for frame structures under earthquake excitation. *J Struct Control Health Monit*. 2014;22(4):707-725. doi:10.1002/stc.1710
3. Gutierrez Soto M, Adeli H. Tuned mass dampers. *Arch Comput Methods Eng*. 2013;20(4):419-431. doi:10.1007/s11831-013-9091-7
4. de Angelis M, Perno S, Reggio A. Dynamic response and optimal design of structures with large mass ratio TMD. *Earthq Eng Struct Dyn*. 2012;41(1):41-60. doi:10.1002/eqe.1117
5. Matta E. Effectiveness of tuned mass dampers against ground motion pulses. *J Struct Eng*. 2013;139(2):188-198. doi:10.1061/(ASCE)ST.1943-541X.0000629
6. Salvi J, Rizzi E. Optimum earthquake-tuned TMDs: seismic performance and new design concept of balance of split effective modal masses. *Soil Dyn Earthq Eng*. 2017;101:67-80. doi:10.1016/j.soildyn.2017.05.029
7. Frahm H, Device for damping vibration of bodies, Inventor. US Patent, 989958. 1909.

8. Lanchester FW. Damping torsional vibrations in crank shafts, Inventor. US Patent, 1085443. 1914.
9. den Hartog JP. *Mechanical Vibrations*. 4th ed. New York (NY), USA: McGraw-Hill; 1956.
10. Housner GW, Bergman LA, Caughey TK, et al. Structural control: past, present, and future. *J Eng Mech*. 1997;123(9):897-971. doi:10.1061/(ASCE)0733-9399(1997)123:9(897
11. Yamamoto M, Sone T. Behavior of active mass damper (AMD) installed in high-rise building during 2011 earthquake off Pacific coast of Tohoku and verification of regenerating system of AMD based on monitoring. *J Struct Control Health Monit*. 2014;21(4):634-647. doi:10.1002/stc.1590
12. Concha A, Thenozhi S, Betancourt RJ, Gadi SK. A tuning algorithm for a sliding mode controller of buildings with ATMD. *Mech Syst Signal Process*. 2021;154:1-21. doi:10.1016/j.ymssp.2020.107539
13. Nagarajaiah S. Adaptive passive, semiactive, smart tuned mass dampers: identification and control using empirical mode decomposition, hilbert transform, and short-term fourier transform. *J Struct Control Health Monit*. 2009;16(7–8):800-841. doi:10.1002/stc.349
14. Lu Z, Wang Z, Zhou Y, Lu X. Nonlinear dissipative devices in structural vibration control: a review. *J Sound Vib*. 2018;423:18-49. doi:10.1016/j.jsv.2018.02.052
15. Lu Z, Wang Z, Masri SF, Lu X. Particle impact dampers: past, present, and future. *J Struct Control Health Monit*. 2018;25(1):1-25. doi:10.1002/stc.2058
16. Matta E. A novel bidirectional pendulum tuned mass damper using variable homogeneous friction to achieve amplitude-independent control. *Earthq Eng Struct Dyn*. 2019;48(6):653-677. doi:10.1002/eqe.3153
17. Smith MC. Synthesis of mechanical networks: the inerter. *IEEE Trans Autom Control*. 2002;47(10):1648-1662.
18. Ma R, Bi K, Hao H. Inerter-based structural vibration control: a state-of-the-art review. *Eng Struct*. 2021;243:1-23. doi:10.1016/j.engstruct.2021.112655
19. Kaveh A, Fahimi Farzam M, Hojat Jalali H. Statistical seismic performance assessment of tuned mass damper inerter. *J Struct Control Health Monit*. 2020;27(10):1-24. doi:10.1002/stc.2602
20. Ikago K, Saito K, Inoue N. Seismic control of single-degree-of-freedom structure using tuned viscous mass damper. *Earthq Eng Struct Dyn*. 2012;41(3):453-474. doi:10.1002/eqe.1138
21. Marian L, Giaralis A. Optimal design of inerter devices combined with TMDs for vibration control of buildings exposed to stochastic seismic excitations. Paper presented at: 11th International Conference on Structural Safety and Reliability, ICOSSAR 2013; New York, NY, 2013. doi:10.1201/b16387-151.
22. Lazar IF, Neild SA, Wagg DJ. Using an inerter-based device for structural vibration suppression. *Earthq Eng Struct Dyn*. 2014;43(8):1129-1147. doi:10.1002/eqe.2390
23. Dai J, Xu ZD, Gai PP. Tuned mass-damper-inerter control of wind-induced vibration of flexible structures based on inerter location. *Eng Struct*. 2019;199:1-15. doi:10.1016/j.engstruct.2019.109585
24. Su N, Xia Y, Peng S. Filter-based inerter location dependence analysis approach of Tuned mass damper inerter (TMDI) and optimal design. *Eng Struct*. 2022;250:1-17. doi:10.1016/j.engstruct.2021.113459
25. Kaveh A, Fahimi Farzam M, Hojat Jalali H, Maroofiazar R. Robust optimum design of a tuned mass damper inerter. *Acta Mech*. 2020;231(9):3871-3896. doi:10.1007/s00707-020-02720-9
26. Petrini F, Giaralis A, Wang Z. Optimal tuned mass-damper-inerter (TMDI) design in wind-excited tall buildings for occupants comfort serviceability performance and energy harvesting. *Eng Struct*. 2020;204:1-16. doi:10.1016/j.engstruct.2019.109904
27. Ruiz R, Taflanidis AA, Giaralis A, Lopez-Garcia D. Risk-informed optimization of the tuned mass-damper-inerter (TMDI) for the seismic protection of multi-storey building structures. *Eng Struct*. 2018;177:836-850. doi:10.1016/j.engstruct.2018.08.074
28. Giaralis A, Taflanidis AA. Optimal tuned mass-damper-inerter (TMDI) design for seismically excited MDOF structures with model uncertainties based on reliability criteria. *J Struct Control Health Monit*. 2018;25(2):1-22. doi:10.1002/stc.2082
29. Wang Z, Giaralis A. Enhanced motion control performance of the tuned mass damper inerter through primary structure shaping. *J Struct Control Health Monit*. 2021;28(8):1-23. doi:10.1002/stc.2756
30. Wang Z, Giaralis A. Top-story softening for enhanced mitigation of vortex shedding-induced vibrations in wind-excited tuned mass damper inerter-equipped tall buildings. *J Struct Eng*. 2021;147(1):1-16. doi:10.1061/(ASCE)ST.1943-541X.0002838
31. Yang Y, Li C. Performance of tuned tandem mass dampers for structures under the ground acceleration. *J Struct Control Health Monit*. 2017;24(10):1-9. doi:10.1002/stc.1974
32. Cao L, Li C. Tuned tandem mass dampers-inerters with broadband high effectiveness for structures under white noise base excitations. *J Struct Control Health Monit*. 2019;26(4):1-17. doi:10.1002/stc.2319
33. Nigdeli SM, Bekdaş G. Optimum tuned mass damper design in frequency domain for structures. *KSCE J Civ Eng*. 2017;21(3):912-922. doi:10.1007/s12205-016-0829-2
34. Sadek F, Mohraz B, Taylor AW, Chung RM. A method of estimating the parameters of tuned mass dampers for seismic applications. *Earthq Eng Struct Dyn*. 1997;26(6):617-635. 10.1002/(SICI)1096-9845(199706)26:6<617::AID-EQE664>3.0.CO;2-Z
35. Bekdaş G, Nigdeli SM. Estimating optimum parameters of tuned mass dampers using harmony search. *Eng Struct*. 2011;33(9):2716-2723. doi:10.1016/j.engstruct.2011.05.024
36. Richiedei D, Tamellin I, Trevisani A. Beyond the tuned mass damper: a comparative study of passive approaches to vibration absorption through antiresonance assignment. *Arch Comput Methods Eng*. 2021;11(3):1-26. doi:10.3390/app11031091
37. Kaveh A. *Applications of Metaheuristic Optimization Algorithms in Civil Engineering*. Springer International Publishing; 2016. doi:10.1007/978-3-319-48012-1.

38. Kennedy J, Eberhart R. Particle swarm optimization. In: Proceeding of the IEEE international conference on neural networks. Perth, Australia. 1995:1942–1948.
39. Kalkan E, Kunnath SK. Effects of fling step and forward directivity on seismic response of buildings. *Earthquake Spectra*. 2006;22(2): 367-390. doi:10.1193/1.2192560
40. Kaveh A, Fahimi Farzam M, Maroofiazar R. Comparing h2 and h∞ algorithms for optimum design of tuned mass dampers under near-fault and far-fault earthquake motions. *Period Polytech Civ Eng*. 2020;64(3):828-844. doi:10.3311/PPci.16389
41. Bhagat S, Wijeyewickrema AC, Subedi N. Influence of near-fault ground motions with fling-step and forward-directivity characteristics on seismic response of base-isolated buildings. *J Earthq Eng*. 2021;25(3):455-474. doi:10.1080/13632469.2018.1520759
42. Pietrosanti D, de Angelis M, Basili M. A generalized 2-DOF model for optimal design of MDOF structures controlled by Tuned Mass Damper Inerter (TMDI). *Int J Mech Sci*. 2020;185:1-15. doi:10.1016/j.ijmecsci.2020.105849
43. Pietrosanti D, de Angelis M, Basili M. Optimal design and performance evaluation of systems with Tuned Mass Damper Inerter (TMDI). *Earthq Eng Struct Dyn*. 2017;46(8):1367-1388. doi:10.1002/eqe.2861

How to cite this article: Fahimi Farzam M, Hojat Jalali H. Tandem tuned mass damper inerter for passive control of buildings under seismic loads. *Struct Control Health Monit*. 2022;29(9):e2987. doi:10.1002/stc.2987

APPENDIX A

The mass, stiffness, and damping matrices along with other relevant information for the TMDI and shown in Equations (A1)–(A5). The inerter contribution is added to the mass matrix, where the elements corresponding to the two end terminals of the inerter are modified by adding b and two off diagonal term equal to $-b$ at their intersections.

$$M = \begin{pmatrix} m_1 & & & & & & \\ & m_2 & & & & & \\ & & \ddots & & & & \\ & & & m_{ib}+b & \cdots & -b & \\ & & & \vdots & \ddots & & \\ & & & & & m_N & \\ & & & -b & & & m_d+b \end{pmatrix}, \tag{A1}$$

$$K = \begin{pmatrix} k_1+k_2 & -k_2 & & & & \\ -k_2 & k_2+k_3 & -k_3 & & & \\ & & \ddots & & & \\ & & -k_N & k_N+k_d & -k_d & \\ & & & -k_d & k_d & \end{pmatrix}, \tag{A2}$$

$$C = \begin{pmatrix} c_1+c_2 & -c_2 & & & & \\ -c_2 & c_2+c_3 & -c_3 & & & \\ & & \ddots & & & \\ & & -c_N & c_N+c_d & -c_d & \\ & & & -c_d & c_d & \end{pmatrix}, \tag{A3}$$

$$X(t) = [x_1 \;\; x_2 \ldots \;\; x_N \;\; x_d]^T, \tag{A4}$$

$$\boldsymbol{h} = [\mathrm{m}_1, \mathrm{m}_2, ..., \mathrm{m}_{n-1}, \mathrm{m}_n, \mathrm{m}_d]^T. \tag{A5}$$

The mass, stiffness, and damping matrices along with other relevant information for the TTMDI and are shown in Equations (A6)–(A10).

$$M = \begin{pmatrix} m_1 & & & & & & & \\ & m_2 & & & & & & \\ & & \ddots & & & & & \\ & & & m_{ib}+b & \cdots & & -b & \\ & & & \vdots & \ddots & & & \\ & & & & & m_N & & \\ & & & & & & m_{d1} & \\ & & & -b & & & & m_{d2}+b \end{pmatrix}, \tag{A6}$$

$$K = \begin{pmatrix} k_1+k_2 & -k_2 & & & & & \\ -k_2 & k_2+k_3 & -k_3 & & & & \\ & \ddots & & & & & \\ & -k_N & k_N+k_{d1}+k_{d2} & -k_{d1} & -k_{d2} & & \\ & & -k_{d1} & k_{d1}+k_{dc} & -k_{dc} & & \\ & & -k_{d2} & -k_{dc} & k_{d2}+k_{dc} & & \end{pmatrix}, \tag{A7}$$

$$C = \begin{pmatrix} c_1+c_2 & -c_2 & & & & & \\ -c_2 & c_2+c_3 & -c_3 & & & & \\ & \ddots & & & & & \\ & -c_N & c_N+c_{d1}+c_{d2} & -c_{d1} & -c_{d2} & & \\ & & -c_{d1} & c_{d1}+c_{dc} & -c_{dc} & & \\ & & -c_{d2} & -c_{dc} & c_{d2}+c_{dc} & & \end{pmatrix}, \tag{A8}$$

$$X(t) = [x_1 \;\; x_2 ... \;\; x_N \;\; x_{d1} \;\; x_{d2}]^T, \tag{A9}$$

$$\boldsymbol{h} = [\mathrm{m}_1, \mathrm{m}_2, ..., \mathrm{m}_{n-1}, \mathrm{m}_n, \mathrm{m}_{d1}, \mathrm{m}_{d2}]^T. \tag{A10}$$